Acta Crystallographica Section D
Biological Crystallography
ISSN 0907-4449

The structure of human recombinant aldose reductase complexed with the potent inhibitor zenarestat

Takayoshi Kinoshita,[a]* Hiroshi Miyake,[a] Takashi Fujii,[a] Shoji Takakura[b] and Toshio Goto[b]

[a]Exploratory Research Laboratories, Fujisawa Pharmaceutical Co. Ltd, 5-2-3 , Tokodai, Tsukuba, Ibaraki 300-2698, Japan, and [b]Medicinal Biology Research Laboratories, Fujisawa Pharmaceutical Co. Ltd, Kashima 2-1-6, Yodogawa-ku, Osaka 532-8514, Japan

Correspondence e-mail: takayoshi_kinoshita@po.fujisawa.co.jp

Received 15 October 2001
Accepted 5 February 2002

PDB Reference: aldose reductase–zenarestat complex, 1iei, r1ieisf.

The crystal structure of the complex of human recombinant aldose reductase (AR) with zenarestat, one of its potent inhibitors, has been solved at 2.5 Å resolution. Zenarestat fits neatly in the hydrophobic active site and induces unique and dramatic conformational changes. For example, the benzene ring of zenarestat occupies a gap in the side chains of Leu300 and Trp111 that interact directly and forms a CH–π interaction in the native holoenzyme. As a result, the benzene ring of the inhibitor and these side chains form a CH–π–π interaction. Such structural information is key to understanding the mode of action of this class of inhibitors and for rational design of better therapeutics.

1. Introduction

Aldose reductase (AR; EC 1.1.1.21) is an NADPH-dependent enzyme that catalyses the reduction of the aldehyde form of compounds to the corresponding alcohols. The enzyme belongs to the family of oxidoreductases that use NADPH as a cofactor and possesses a broad substrate specificity for various aldo–keto compounds. Although its role in the cell is not clearly defined, it is known to catalyze an important step of the polyol pathway of glucose metabolism.

Clinical interest in AR has resulted from its role in reducing glucose to sorbitol. Enhanced flux of glucose through the polyol pathway is believed to be related to a number of diabetic complications, including neuropathy, nephropathy, cataracts and retinopathy. A large number of inhibitors have been and continue to be developed and some have shown promise in the treatment of diabetic complications. The main structural features of these inhibitors are a polar head group and a hydrophobic ring system (Lee *et al.*, 1994). As shown by crystal structures, whilst the hydrophobic moiety interacts with the hydrophobic cleft of the active site, the polar head group interacts with protein residues that are essential for catalysis.

As one of the promising inhibitors of this enzyme, zenarestat (Fig. 1), 3-(4-bromo-2-fluorobenzoyl)-7-chloro-3,4-dihydro-2,4-dioxo-1(2H)-quinazolineacetic acid, has been reported to inhibit cataract formation and to counteract reduced motor nerve conduction velocity in streptozotocin-

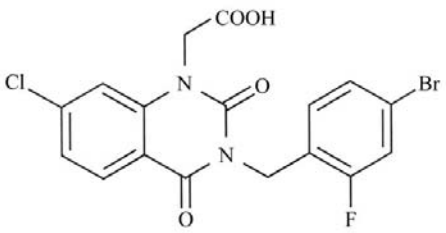

Figure 1
Two-dimensional formula of the inhibitor zenarestat.

induced diabetic rats (Ao *et al.*, 1991). Recently, it has been demonstrated that zenarestat improved both nerve conduction velocity and nerve morphological changes in patients with diabetic peripheral polyneuropathy (Greene *et al.*, 1999). Zenarestat displays an IC_{50} of 44 n*M* for AR and also exhibits excellent pharmacokinetic properties in humans and is currently in phase III clinical studies (Takakura *et al.*, 2002).

A number of quite different conformations of human AR have already been reported (Calderone *et al.*, 2000; Harrison *et al.*, 1994, 1997; Wilson *et al.*, 1992, 1993). Of particular note, the hydrophobic cleft of the active site has a high flexibility corresponding to the broad specificity for substrates and inhibitors. This flexibility results in dramatic movements and each conformation can form one of three different crystal forms: triclinic, monoclinic and orthorhombic. Since zenarestat belongs to a novel structural class of AR inhibitors, we could not predict *a priori* the crystal form or the binding mode in detail. Careful observation of the structure of a complex of AR and zenarestat is essential to understanding the mode of action of this class of inhibitors and for rational design of better therapeutics. Here, we report the structure of AR complexed with zenarestat.

Table 1
Data-collection and refinement statistics of the complex between zenarestat and AR.

Values in parentheses are for the highest resolution shell (2.60–2.50 Å).

Data collection and processing	
Unit-cell parameters (Å, °)	a = 40.37, b = 47.69, c = 47.94, α = 76.0, β = 67.5, γ = 76.7
Diffraction data	
d_{min} (Å)	2.5
Unique reflections	10335
R_{sym} (%)	6.0 (9.1)
Completeness (%)	94.6 (83.7)
Redundancy	2.2 (2.1)
$I/\sigma(I)$	17.7 (16.7)
Rigid-body refinement	
Resolution (Å)	8.0–4.0
R_{cryst} (%)	27.4
Refinement	
Resolution (Å)	8.0–2.5
Reflections used [$F > 2\sigma(F)$]	9831
R_{cryst}/R_{free} (%)	17.8/19.9 (19.7/22.7)
Final model	
Protein residues	316
Coenzyme	1
Inhibitor	1
Water	186
R.m.s. deviations	
Bonds (Å)	0.039
Angles (Å)	4.4
Dihedrals (Å)	29.8
Mean B factors (Å^2)	
Protein	11.6
$NADP^+$	11.8
Zenarestat	9.1
Water	18.8

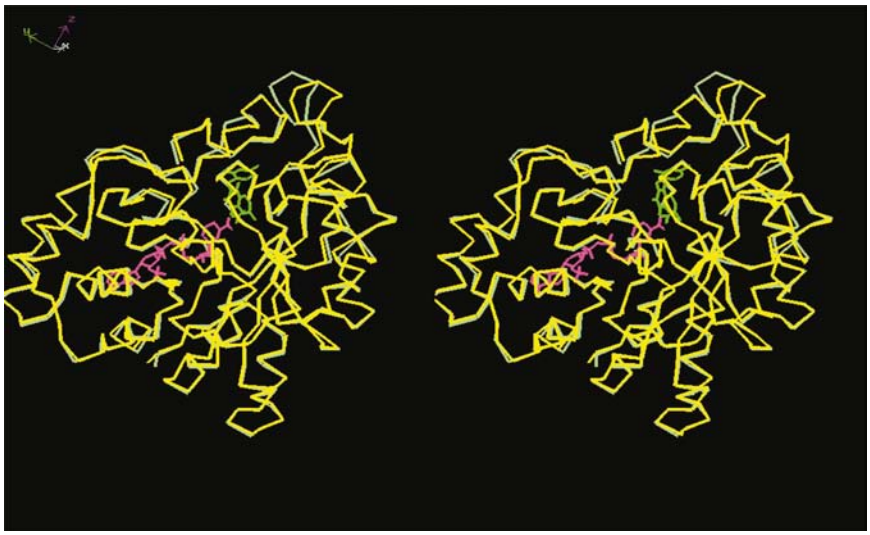

Figure 2
A stereoview of superimposed C^{α} backbone structures of the complex with zenarestat (yellow, holoenzyme; pink, NADPH; green, zenarestat) and of the holoenzyme 1mar (white). The two holoenzyme molecules have almost the same backbones, except for the loop on the upper right of the active site.

2. Materials and methods

2.1. Crystallization

Human recombinant AR was purchased from Wako Pure Chemical Industries Ltd and zenarestat was prepared at our company. The protein solution was used for crystallization with no further purification and was employed at 14 mg ml^{-1} in 50 m*M* citrate buffer pH 5.0 and 7 m*M* 2-mercaptoethanol with 1 m*M* zenarestat suspended. All crystallization trials were carried out by the hanging-drop method of vapour diffusion by mixing 2 µl of the protein solution with 2 µl of the reservoir solution and equilibrating the drops over the reservoir at room temperature.

All published reports describe AR as crystallizing using the same precipitant at the same pH: polyethylene glycol 6000 at pH 5.0, although those crystals can be classified into three crystal forms. Therefore, the first trial was performed using grid sceening referred to the conditions for crystallization in these reports: 15–25%(*w*/*v*) polyethylene glycol 6000, 50 m*M* citrate buffer pH 5.0. Finally, the crystals of human AR complexed with zenarestat used for data collection were grown against reservoirs containing 20–22.5%(*w*/*v*) polyethylene glycol 6000 in 50 m*M* citrate buffer pH 5.0. The crystals grew to maximum dimensions of approximately 0.15 × 0.10 × 0.05 mm in 2 weeks.

2.2. Data collection and refinement

After dipping in a solution of Paratone-N (Hampton Research Inc.), X-ray diffraction data were collected at 100 K using synchrotron facilities (Sakabe, 1991) at beamline BL6B of the Photon Factory, Japan for the Structural Biology Sakabe Project. The crystal-to-imaging plate distance was 573 mm and the oscillation

range was 7°. The image data were processed using *DENZO* (Otwinowski, 1997) and *SCALEPACK* (Fox & Holmes, 1966) (Table 1).

The structure of human AR complexed with zenarestat was solved by the molecular-replacement method using the *AMoRe* program (Navaza, 1993) from the *CCP*4 suite (Collaborative Computational Project, Number 4, 1994). This complex crystallized in the triclinic form, with similar unit-cell parameters to that registered as 1mar (Wilson *et al.*, 1993) in the Protein Data Bank (PDB). However, because only the atomic coordinates of the C^{α} atoms were available for 1mar, the holoenzyme of the orthorhombic form (PDB code 1ads) was used as a search model for structure solution. After a rigid-body refinement, the zenarestat molecule was placed in the electron density by a Fourier difference map. The model of the complex was used as the starting point of the refinement, which included a rigid-body refinement step, a slow-cooling step, Powell minimization and a temperature-factor refinement. Water molecules were then placed in a difference map (2σ level) and minimization was performed. The programs *X-PLOR* (Brünger, 1992), *QUANTA* (Molecular Simulations, Inc.) and *X-SOLVATE* (Molecular Simulations, Inc.) were used for refinement, model building and picking of water molecules, respectively.

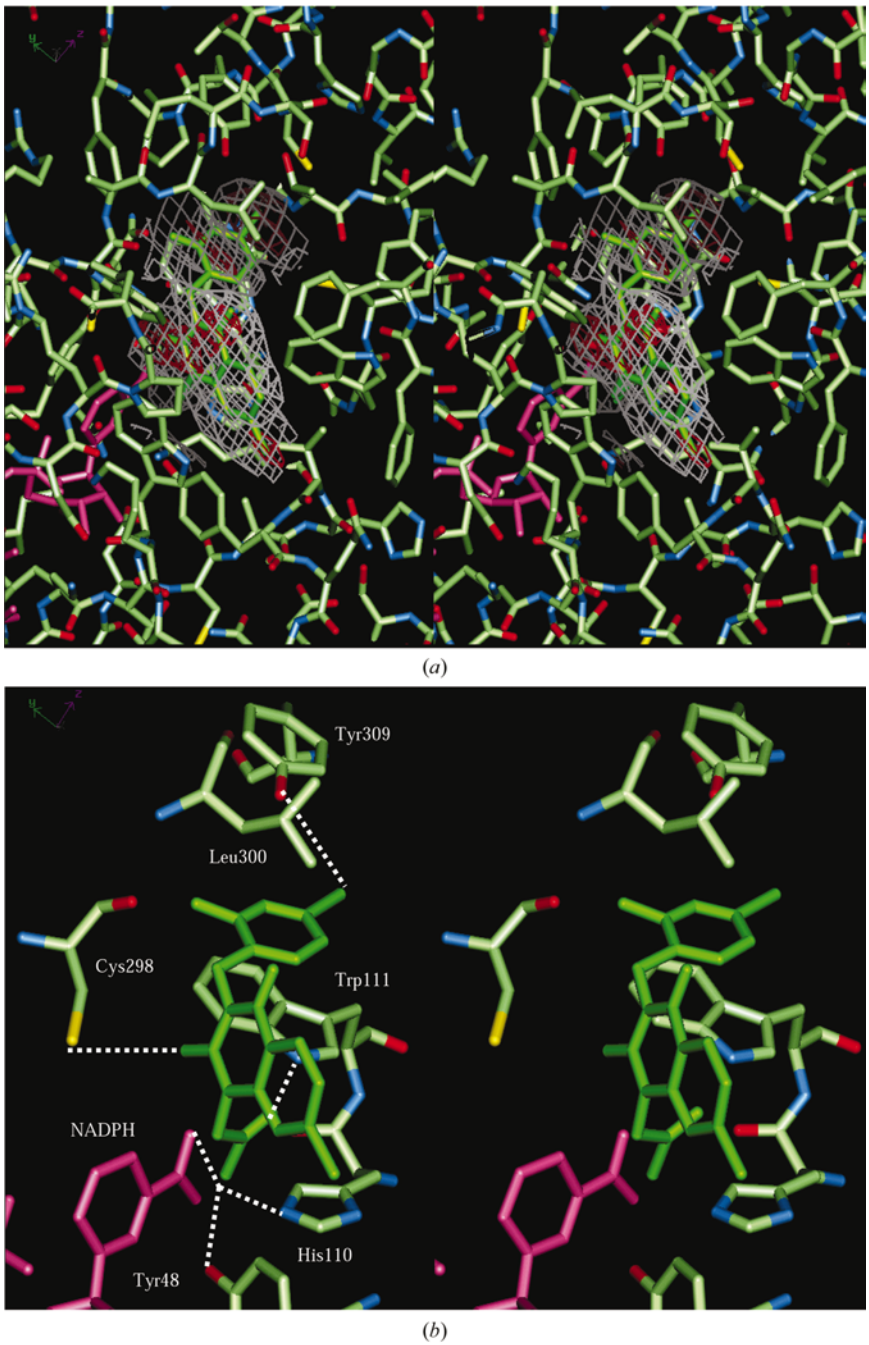

Figure 3
Stereoviews of the active site (green, zenarestat; pink, NADPH; red, O atoms; blue, N atoms; yellow, S atoms; white, C atoms). (*a*) The inhibitor is enclosed in a wire-cage representation of the electron-density map calculated at 2.5 Å resolution by a Fourier transform using $|F_o| - |F_c|$ as coefficients (grey line, 1σ level map; red line, 3σ level map). F_c values calculated from the initial protein structure. The electron density at heavy-atom positions (Br, Cl) and two carbonyl groups of the quinazoline ring is higher than that of the other atoms of the inhibitor. (*b*) Zenarestat makes six hydrogen bonds with AR. The hydrogen bonds are displayed as the white dotted lines.

3. Results and discussion

As mentioned above, this complex crystallized in a triclinic form with similar unit-cell parameters to the complex with the inhibitor zopolestat (PDB code 1mar). Thus, the C^{α} backbone structures of holoenzyme in the two complexes are very similar to each other, with an r.m.s.d. value of 0.59 Å (Fig. 2), although the two-dimensional formulae of these inhibitors are different. Both inhibitors occupied almost the same site in the respective complexes. However, the detailed structures of these complexes, such as the inhibitor-induced conformational change of the side chains, are quite different. Therefore, careful and precise observation of the active site is required to provide hints for effective modification of this class of inhibitors.

Bound zenarestat, with its unambiguous difference electron-density map (Fig. 3*a*), occupies almost the entire active-site cleft at the top of the β-barrel (Fig. 2). The bound inhibitor is almost buried in the active-site cavity; it has an accessible surface area of 46.8 $Å^2$, 8.0% of the total surface area of the unbound inhibitor. The binding mode indicated many features consistent with its potent inhibition. The quinazoline ring is almost at a right angle to and bisects the

plane of the benzene ring, protruding from the centre of the pocket. It is also perpendicular to the nicotinamide ring of NADPH.

There is excellent complementarity between bound zenarestat and the active site of AR. The inhibitor makes an unusually large number of contacts with the active site, totalling 110 contacts within a 4 Å distance: 92 with 13 residues, 15 with the nicotinamide moiety of NADPH and three with three ordered water molecules. The hydrophilic head makes a network of hydrogen bonds to the catalytic site (Fig. 3*b*). That is, one acid O atom forms three hydrogen bonds with His110 $N^{\varepsilon 2}$ (2.6 Å), Tyr48 O^{η} (2.9 Å) and the carbonyl O atom of NADPH (2.6 Å). The other O atom forms a hydrogen bond with Trp111 $N^{\varepsilon 1}$ (2.9 Å). The two carbonyl O atoms of the quinazoline ring make hydrogen bonds with a side chain of AR and a water molecule, respectively. The 2-carbonyl O atom of the ring forms a hydrogen bond with Cys298 S^{γ} (3.5 Å) and the 4-carbonyl O atom with water127 (2.8 Å). The hydrophobic moiety, including the two ring systems of the inhibitor, binds to the hydrophobic active site consisting of 11 amino acids: Trp20, Val47, Trp79, His110, Trp111, Thr113, Phe121, Phe122, Tyr219, Ala299 and Leu300. The benzene ring of zenarestat cuts into the side chains of Leu300 and Trp111 that interact directly and form a CH–π interaction in the native holoenzyme (Fig. 4*a*). As a result, these two side chains and zenarestat form a quite unique CH–π–π interaction (Fig. 4*b*). The benzene ring forms a π–π interaction with the indole ring of Trp111 and a CH–π interaction with the methyl group of Leu300. The other induced fitting is found at the amino acids near the Br atom of bound zenarestat, where the side chains were found to be moved significantly (Tyr309 OH, 4.7 Å; Phe115 C^{ζ}, 4.3 Å). Consequently, the Br atom forms a hydrogen bond to Tyr309 OH (3.4 Å). These inhibitor-induced conformational changes indicate why the selectivity of the hydrophobic site is very broad.

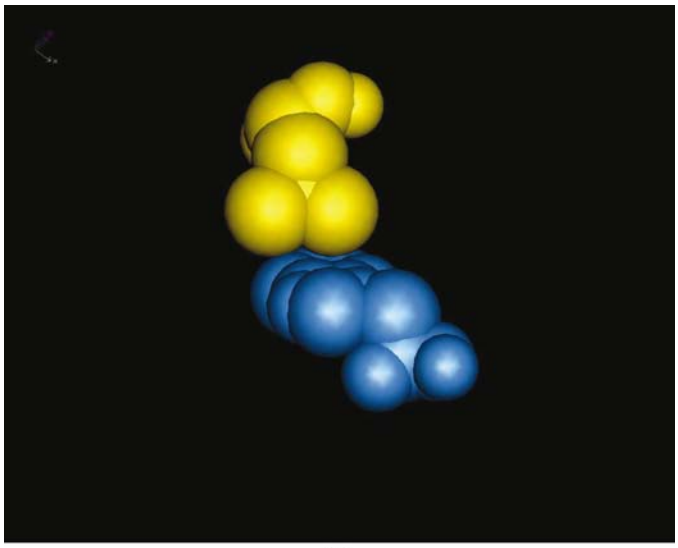

(*a*)

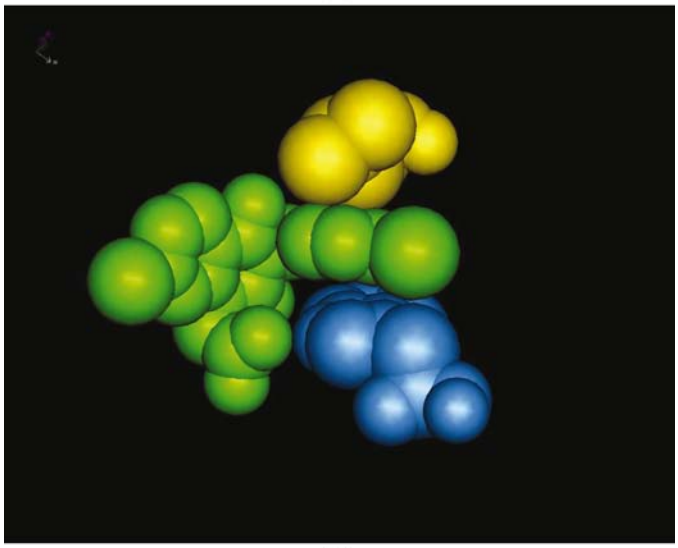

(*b*)

Figure 4
Space-filled models. (*a*) The side chains of Leu300 (yellow) and Trp111 (blue) make a CH–π interaction in the native holoenzyme. (*b*) The benzene ring of zenarestat (green) and the two upper side chains form a CH–π–π interaction in this complex.

4. Conclusions

In the crystal structures solved so far, including this complex, the portion binding the polar head group of the inhibitor is structurally stable. Therefore, considering this portion of these inhibitors as a rigid template, the polar head part may be readily modified. The high flexibility of the hydrophobic part, however, makes it difficult to design the hydrophobic part of an inhibitor. We believe that the structural information reported here should be helpful for major improvement of several properties of this class of inhibitors which are essential for its success as a medicine; for example, solubility in water, toxicity and metabolism. However, it is noted that if major structural modification is examined, it is recommended to certify the enzyme–inhibitor interaction by X-ray analysis.[1]

[1] Supplementary data have been deposited in the IUCr electronic archive (Reference: gr2214). Services for accessing these data are described at the back of the journal.

We would like to thank Dr N. Sakabe of the Structural Biology Sakabe project for data collection. We also would like to thank Drs D. Barrett and I. Nakanishi for helpful discussion and critical evaluation of the manuscript.

References

Ao, S., Kikuchi, C., Ono, T. & Notsu, Y. (1991). *Invest. Ophthalmol. Vis. Sci.* **32**, 3078–3083.
Brünger, A. T. (1992). *X-PLOR Version* 3.1. *A System for X-ray Crystallography and NMR.* New Haven, Connecticut, USA: Yale University Press.
Calderone, V., Chevrier, B., van Zandt, M., Lamour, V., Howard, E., Poterszman, A., Barth, P., Mitschler, A., Lu, J., Dvornik, D. M., Klebe, G., Kraemer, O., Moorman, A. R., Moras, D. & Podjarny, A. (2000). *Acta Cryst.* D**56**, 536–540.
Collaborative Computational Project, Number 4 (1994). *Acta Cryst.* D**50**, 760–763.

Fox, G. C. & Holmes, K. C. (1966). *Acta Cryst.* **20**, 886–891.
Greene, D. A., Arezzo, J. C. & Brown, M. B. (1999). *Neurology*, **53**, 580–591.
Harrison, D. H., Bohren, K. M., Ringe, D., Petsko, G. A & Gabbay, K. (1994). *Biochemistry*, **33**,2011–2020.
Harrison, D. H. T., Bohren, K. M., Petsko, G. A., Ringe, D. & Gabbay, K. H. (1997). *Biochemistry*, **36**, 16134–16140.
Lee, Y. S., Pearlstein, R. & Kador, P. F. (1994). *J. Med. Chem.* **37**, 787–792.
Navaza, J. (1993). *Acta Cryst.* D**49**, 588–591.
Otwinowski, Z. (1997). *Methods Enzymol.* **276**, 307–326.
Sakabe, N. (1991). *Nucl. Instrum. Methods A*, **303**, 448–463.
Takakura, S., Minoura, H., Shimoshige, Y., Minoura, K., Kawamura, I., Fujiwara, T., Saitoh, T., Shimojo, F., Seki, J. & Goto, T. (2002). In the press.
Wilson, D. K., Bohren, K. M., Gabbay, K. H. & Quiocho, F. A. (1992). *Science*, **257**, 81–84.
Wilson, D. K., Tarle, I., Peterash, J. M. & Quiocho, F. A. (1993). *Proc. Natl Acad. Sci. USA*, **90**, 9847–9851.